A GEOMECHANICAL APPROACH TO EVALUATE BRITTLENESS USING WELL LOGS: MISSISSIPPIAN LIMESTONE, NORTHERN OKLAHOMA

by

JAMES MARTIN

Presented to the Faculty of the Graduate School of
The University of Texas at Arlington in Partial Fulfillment
of the Requirements
for the Degree of

MASTER OF SCIENCE IN GEOLOGY

THE UNIVERSITY OF TEXAS AT ARLINGTON

May 2015

Acknowledgements

There were many people that supported me in the process of achieving this accomplishment and to each of them I would like to offer my sincerest appreciation. I want to thank the faculty and staff of the Department of Earth and Environmental Sciences at the University of Texas at Arlington for providing an environment where I could be challenged yet all of the tools needed to be successful were made available. A heartfelt thank you to my advisor Dr. John Wickham for allowing me the opportunity to learn from and be guided by you through this process. I feel so fortunate to have had the opportunity to work with such an outstanding professor and mentor. I would like to thank the members of my committee, Dr. Xinbao Yu and Dr. Richard McMullen, for the time that you took to follow and review my work. I would like to thank Fairway Resources for being so generous and allowing access to the data necessary for the completion of this thesis. To my wife Erin, you have my deepest love and gratitude for never wavering in your support of me through this process. You are my best friend and the most amazing mother to our son, Wesley.

April 10, 2015

Abstract

A GEOMECHANICAL APPROACH TO EVALUATE

BRITTLENESS USING WELL LOGS:

MISSISSIPPIAN LIMESTONE,

NORTHERN OKLAHOMA

JAMES MARTIN, M.S.

The University of Texas at Arlington, 2015

Supervising Professor: John Wickham

Fracture density, or brittleness, of a rock is an important factor in understanding the characteristics of a reservoir and the reservoir's predisposition to fracturing. This becomes particularly critical when exploring and producing in tight or fracture dominated reservoirs such as that of the Mississippian limestone in the study area on the Northern Shelf of the Anadarko basin, Oklahoma. Previous work has defined brittleness on the basis of mineralogy or elastic rock parameters. This study explores a new definition of brittleness based on geomechanical principles that incorporates linear elastic rock properties as well as fracture toughness. The equation being used for this purpose was derived from a relationship published by Sih (1985). According to Sih, "*the surface and volume energy density of each material element are related by the rate of change of volume with surface*." This would suggest that $(F_d)(Ua) = Uv$, where F_d is the fracture density (fracture surface/volume); U_a is the energy needed to create fracture area A (related to surface energy density); and U_v is the strain energy density.

Data gathered from acoustic, density, and micro-resistivity image logs taken from two vertical wells drilled through the Mississippian formation in Northern Oklahoma were used to create and attempt to validate a brittleness log based on the new equation. The equation assumes linear elasticity, and mode I fracturing. Based on these assumptions, the equation relates fracture density, or brittleness, to K_{IC}, (the critical fracture toughness for mode I fractures), Young's Modulus, shear modulus, Poisson's Ratio, and the strain state.

The resulting brittleness log created from this equation is compared to brittleness logs derived from other methods of determining brittleness from well logs and checked against the fracture frequency observed from image log data. This more comprehensive method of determining brittleness could aid in developing a more effective approach to reservoir characterization and in improved targeting of brittle intervals within a formation.

Table of Contents

List of Figures

List of Tables

Chapter 1

Introduction

A material is considered brittle if, when subjected to stress, it breaks without significant deformation (strain) (Song et al., 2014). This would imply a relationship between brittleness and fracture density. In a stratified layer of rock, subjected to constant strain, the more brittle layers would have a higher observed fracture density. In turn, rocks that exhibit less fracturing under the same constant strain would indicate a more ductile zone, which may not be as amenable to propagating or maintaining a fracture.

In unconventional reservoirs, formations exhibiting low primary porosity and permeability, the need to have a method of determining zones of higher brittleness becomes necessary. In formations with lower primary porosities, permeability is enhanced by hydraulic stimulation. The ability to target brittle layers and increase permeability through hydraulic fracturing allows operators to make economic discoveries in fields that were once uneconomic.

There are both conventional and unconventional components to the Mississippian reservoirs of the mid-continent. The historically produced conventional component, informally called the “chat,” is a high porosity low resistivity interval (Watney et al., 2001); where present, it occurs at the top of the Mississippian section beneath the Mississippian and Pennsylvanian unconformity. Mississippian chat reservoirs have been exploited for decades with vertical wells. The chat interval ranges from 0 m to 100 feet in the study area, while the average thickness of the Mississippian section is around 500 feet. The unconventional or “tight lime” interval of the Mississippian was until recently bypassed as uneconomic. These zones are described as low-porosity, partially dolomitized cherty limestone that has low permeability (Brevetti et, al., 1985).

The unconventional interval is highly fractured with most of the porosity and permeability being contributed by the fractures (Brevetti et, al., 1985). Brevetti et al. suggest that the origin of the fracturing is due to structural flexures, proximity to faulting, and differential compaction. With the advent of horizontal drilling and hydraulic stimulation methods, the high angle fractures in this area were able to be connected forming large fracture networks that make these wells economic. Fracture density, in most cases, will determine the reservoir's value (Ward 1965). One of the challenges then becomes identifying intervals that are considered brittle.

Well log data from three wells, Reitz #1 and #2 (Alfalfa County), and Scribner #1(Woods county), drilled through the Mississippian section, were made available to test a new equation that predicts fracture density, or brittleness (Figure 1). This brittleness equation was used for this study to identify brittle and ductile zones within the Mississippian in the area of Woods and Alfalfa counties, Oklahoma. The resulting log may be a more effective indicator of brittle zones. These zones may also be mechanically compartmentalized, i.e. be bound by ductile zones that act as fracture barriers. An understanding of the rock mechanical properties of the Mississippian is critical to effectively exploit the Mississippian unconventional or "tight lime" unit.

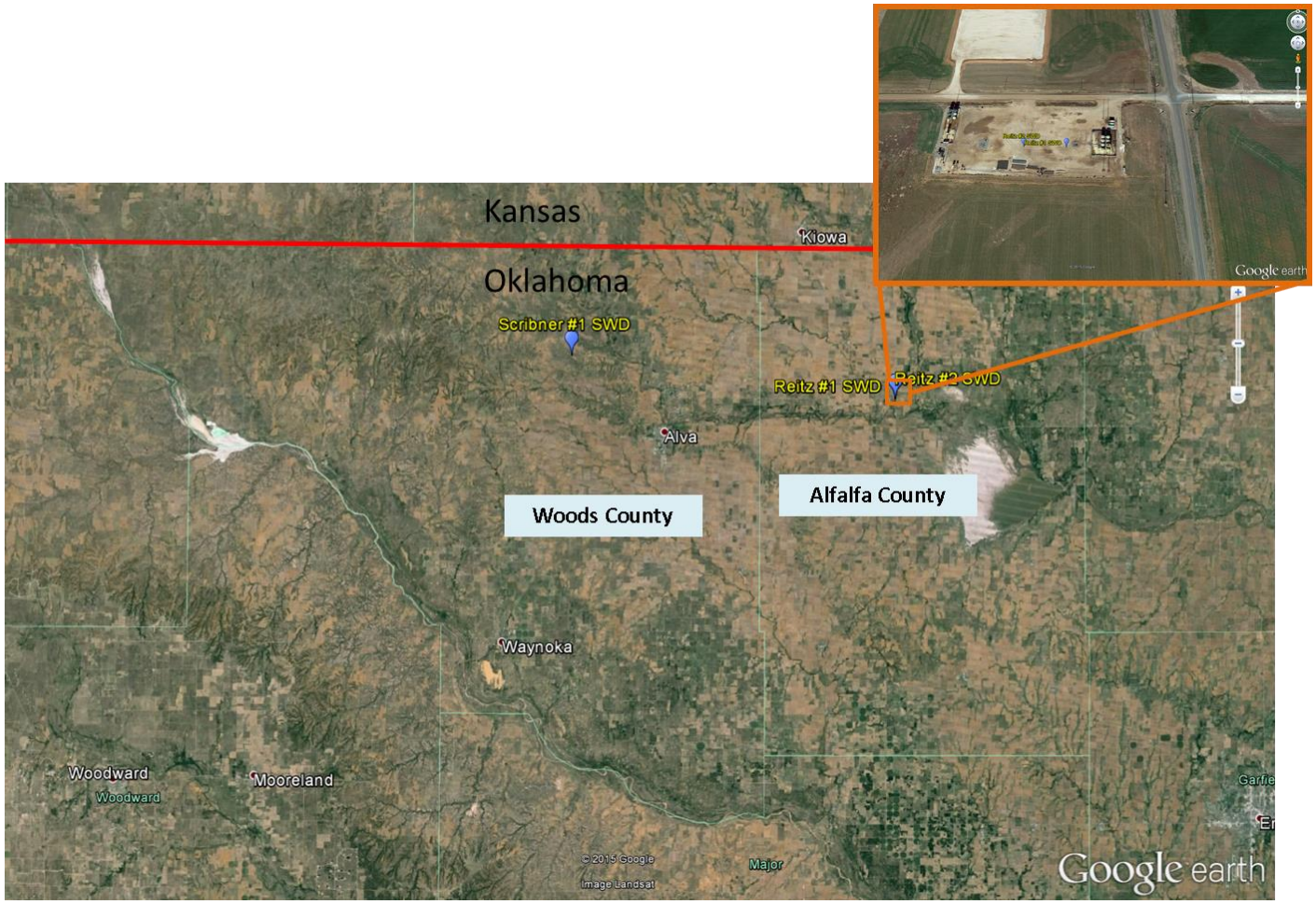

Figure 1 Satellite image of well locations in Woods and Alfalfa counties, northern Oklahoma

Chapter 2

Geologic Setting

2.1 Structural Influences and Features

According to Perry (1989) the history of the Anadarko Basin region can be divided into four periods. The first phase occurred during the middle Proterozoic and involved crustal consolidation and regional high grade metamorphism. This was followed by a Late Precambrian to Middle Cambrian rifting phase. Due to cooling and subsidence that occurred at the end of the rifting phase, the Southern Oklahoma Trough was formed representing the third phase of the Anadarko Basin development. The final phase was a Late Mississippian (Chesterian) plate collision between North America and Gondwana or an intervening microplate leading to the Ouchita orogeny as well as the ancestral Rocky Mountains (Kluth 1986). As a result of this tectonic event, the Nemaha uplift, a major Precambrian structural feature to the east of the study area, was reactivated (Dolton et al., 1989). The Nemaha uplift separates the Anadarko Basin from the Cherokee platform to the east. According to Berendsen and Blair (1986) the Nemaha Uplift had left-lateral wrench fault component caused by plate collision along the continental margin. Figure 2 (lane and De Keyser, 1980) shows the paleogeographic features of the mid-contintent during Mississippian time. Figures 3 and 4 (Johnson 2008) illustrates the current day major structural features of Oklahoma. Other structural features, in the study area are small-scale, low relief anticlines. Primary trapping mechanisms therefore are represented by stratigraphic pinch outs.

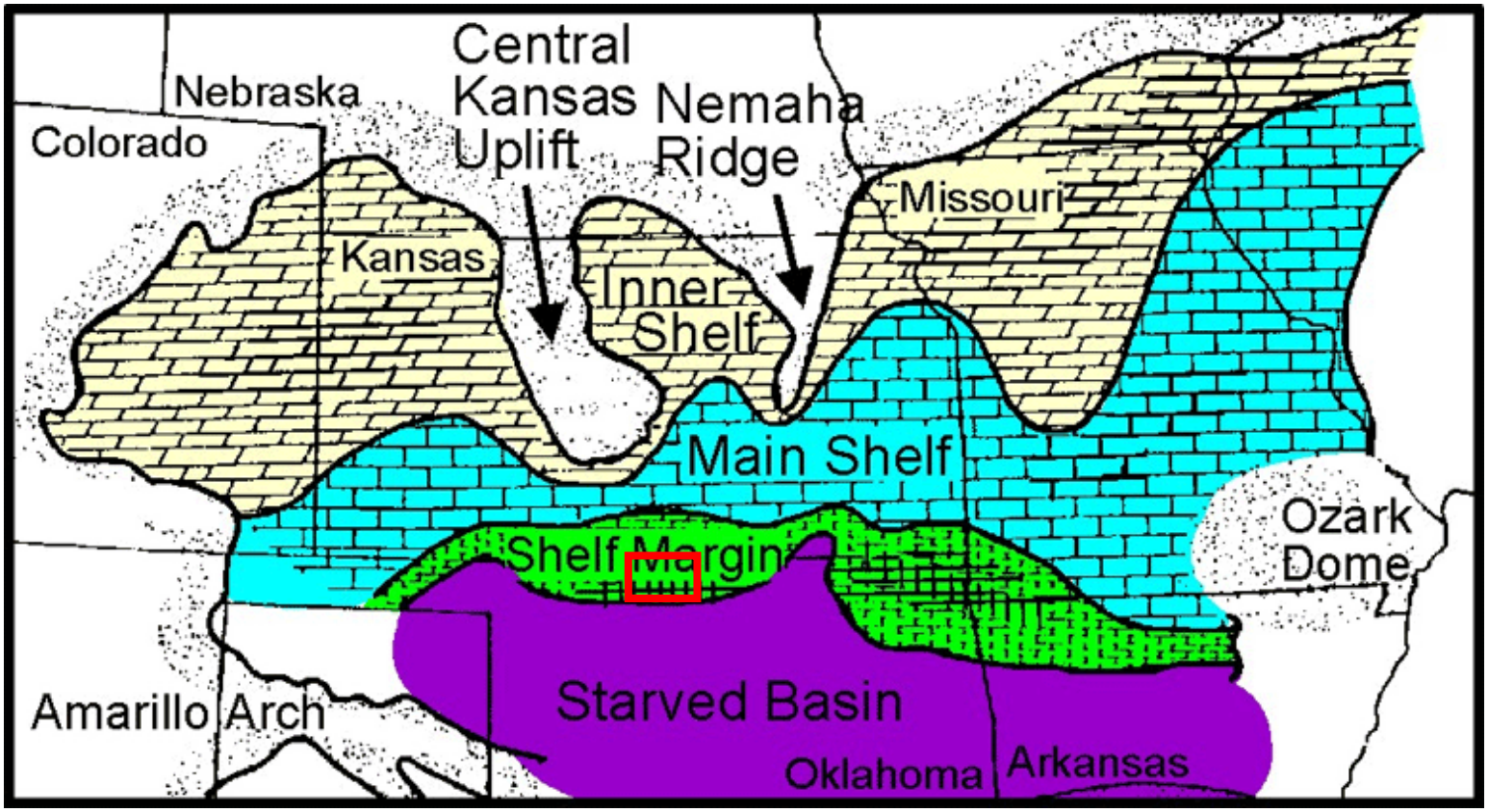

Figure 2 Map of paleo geographic features of the mid-continent during Mississippian time. Red square indicates study area (modified from Lane and De Keyser, 1980)

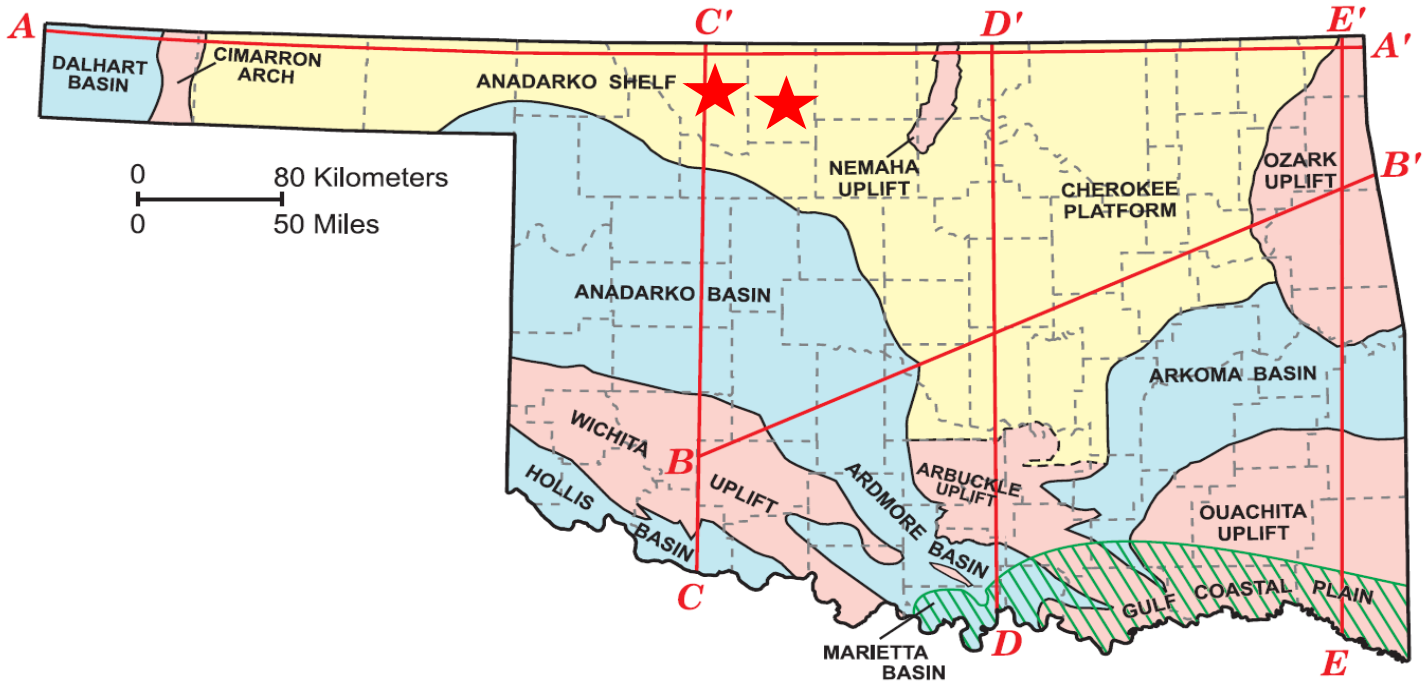

Figure 3 Major structural provinces of Oklahoma. Red stars indicate approximate location of study wells in Woods and Alfalfa counties (Johnson 2008)

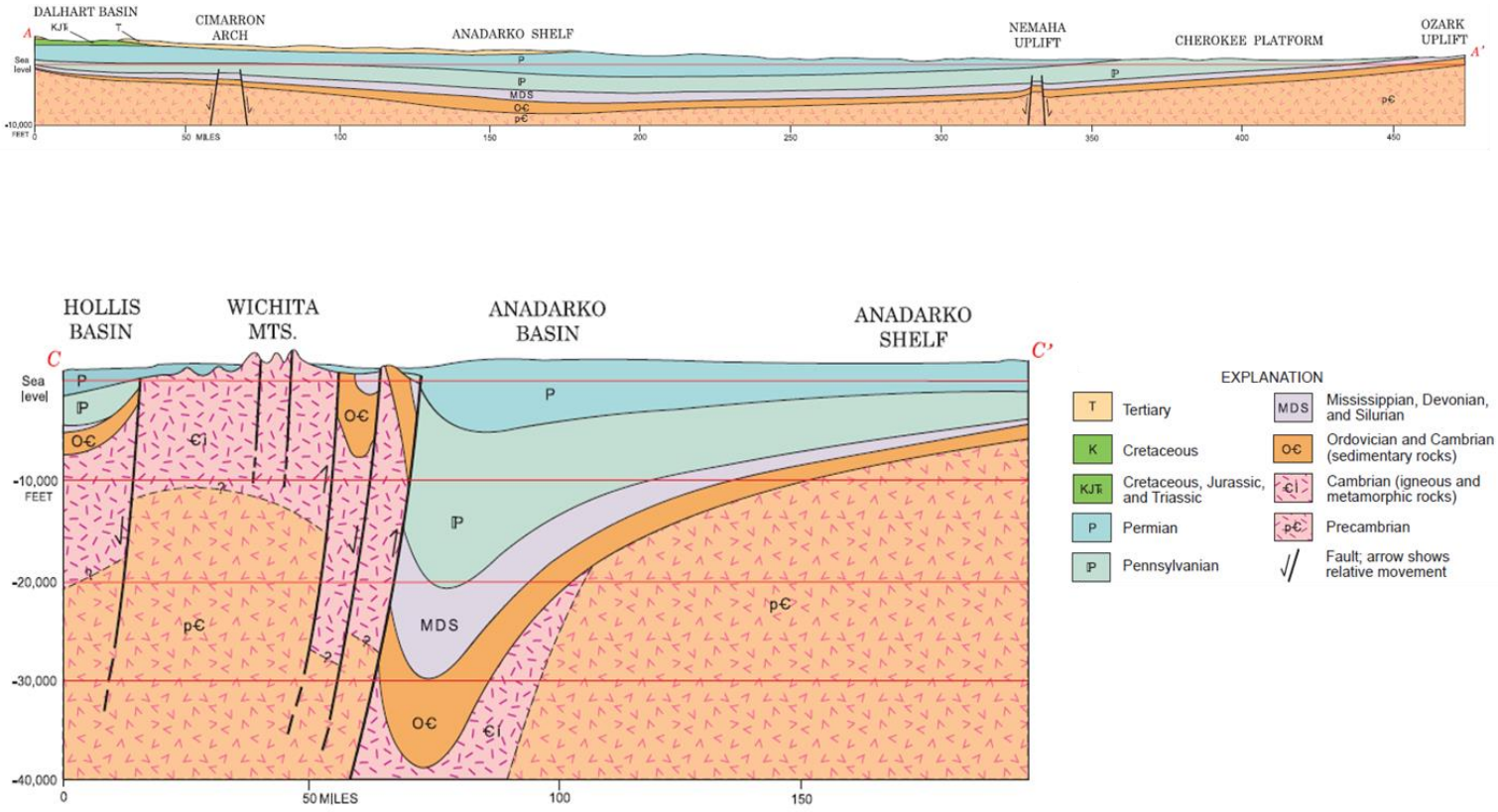

Figure 4 East-West cross section (A-A') and North-South cross section (C-C'), through the study area illustrating major structural elements in the subsurface (Johnson 2008)

2.3 Stratigraphy

Correlating stratigraphy from the Mississippian outcrop to the subsurface in north-central Oklahoma and south-central Kansas raises several issues according to Cahill (2012). For instance, there are both formal and informal names used for intervals in both the outcrop and subsurface. Another problem is that correlations are made by both lithostratigraphic and chronostratigraphic methods. Finally, Cahill notes that there is approximately 200 miles between the Mississippian outcrop and the subsurface where correlations based on subsurface techniques are done.

During Mississippian time the study area lied along the shelf margin of the Anadarko Basin (Figure 2). Informally, the Mississippian section in the study area is divided into the Kinderhook Formation, St. Joe Group, Mississippian Dense and the "Mississippian chat". The St. Joe Group is further subdivided into the Compton Formation, Northview Formation and the Pierson Formation. The Pierson Formation is not present in the study wells so is not included in this work. Johnson (1998), describes Early Mississippian deposition of oolitic fossiliferous crinoidal limestones interbedded with shales and siltstones. He suggests that chert, observed mainly in Osagean and Meramecian rocks, replaces ten to thirty percent of the carbonate. The "Mississippian chat" was produced within 100 feet of the top of the Mississippian section in north central Oklahoma and is described as a zone of rubble consisting of limestone, weathered chert, fractured siliceous limestone and tripolitic chert (Smith 1989). The "chat" was formed during a period of aerial exposure between Mississippian time and Pennsylvanian time; sea level rise in early Pennsylvanian time buried the unconformity. The lithostratigraphic method is used to descibe the subsurface formations of the Mississippian in the study area (Figure 5). Figures 6 illustrates the porosity, gamma ray, PE, and deep resistivity

logs that characterize the subsurface formations within the Mississippian section for the Reitz #2 SWD and the Scribner #1 SWD wells.

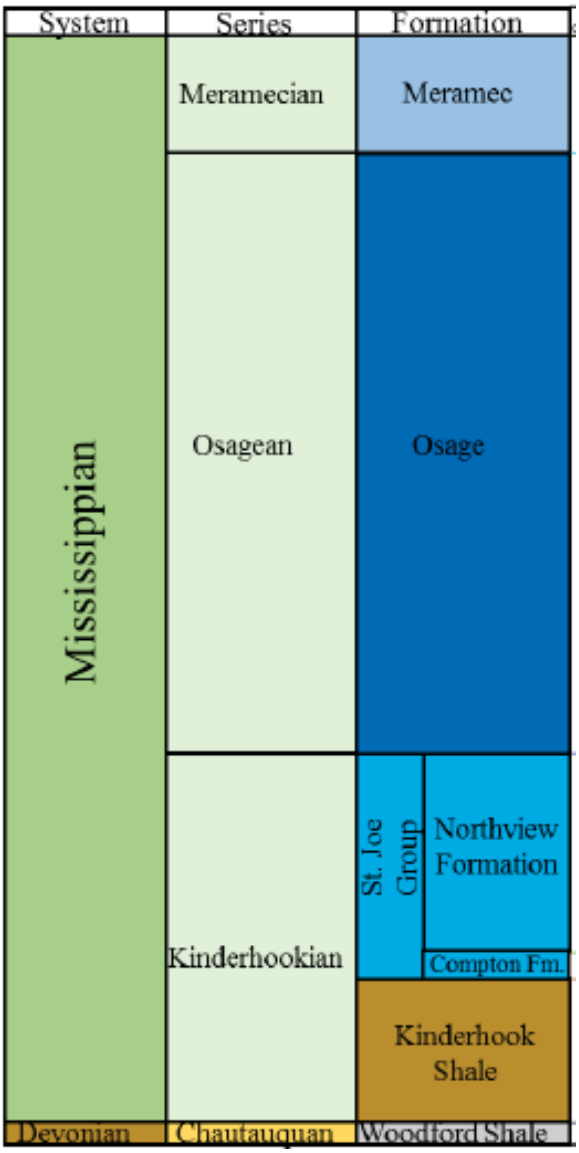

Figure 5 Stratigraphic section of study area (Cahill 2012)

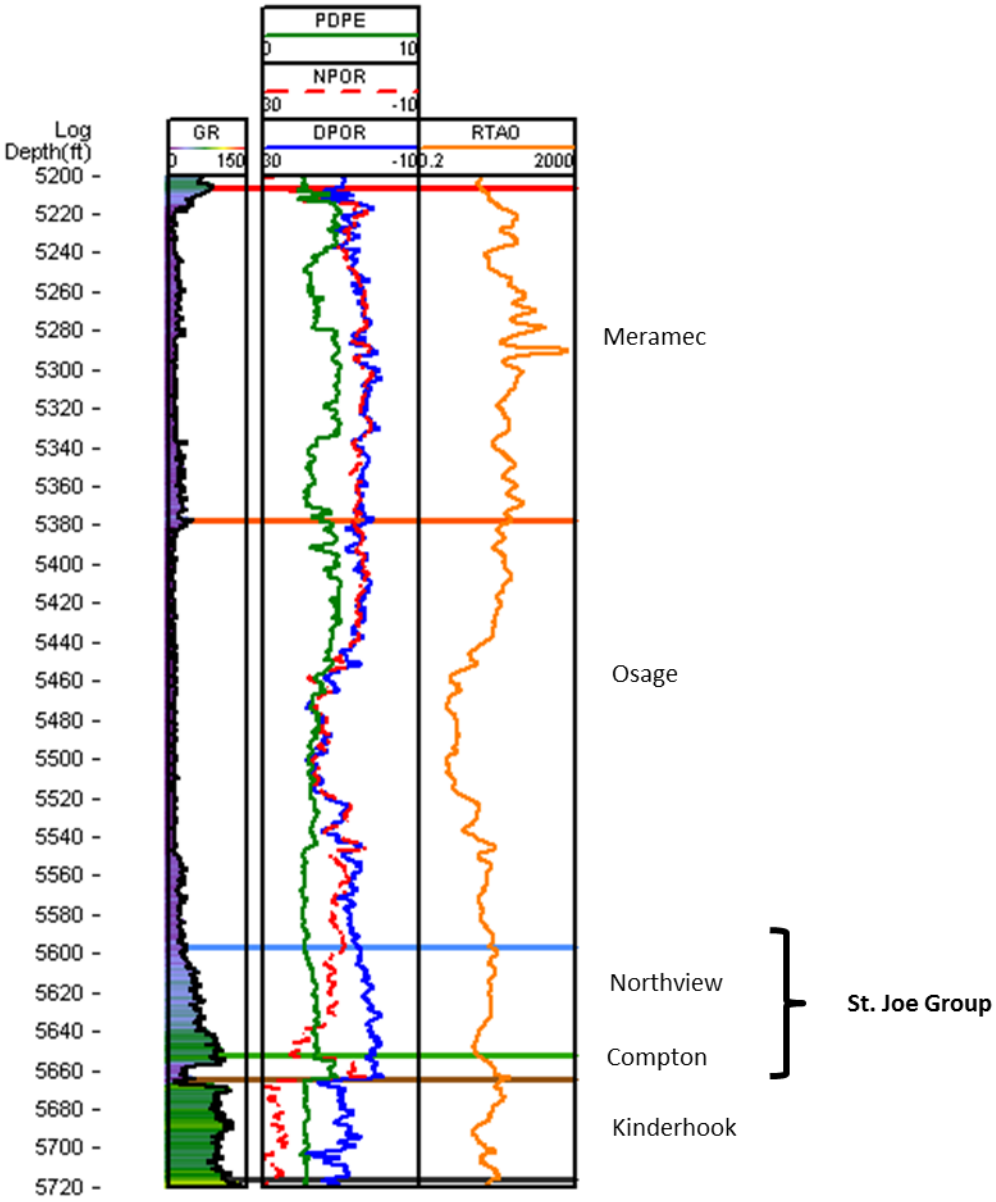

Figure 6 Log curves through the Mississippian series for the Reitz #2 SWD. GR = gamma ray, PDPE = photo electric effect, NPOR = neutron porosity, DPOR = density porosity, RTAO = deep resistivity

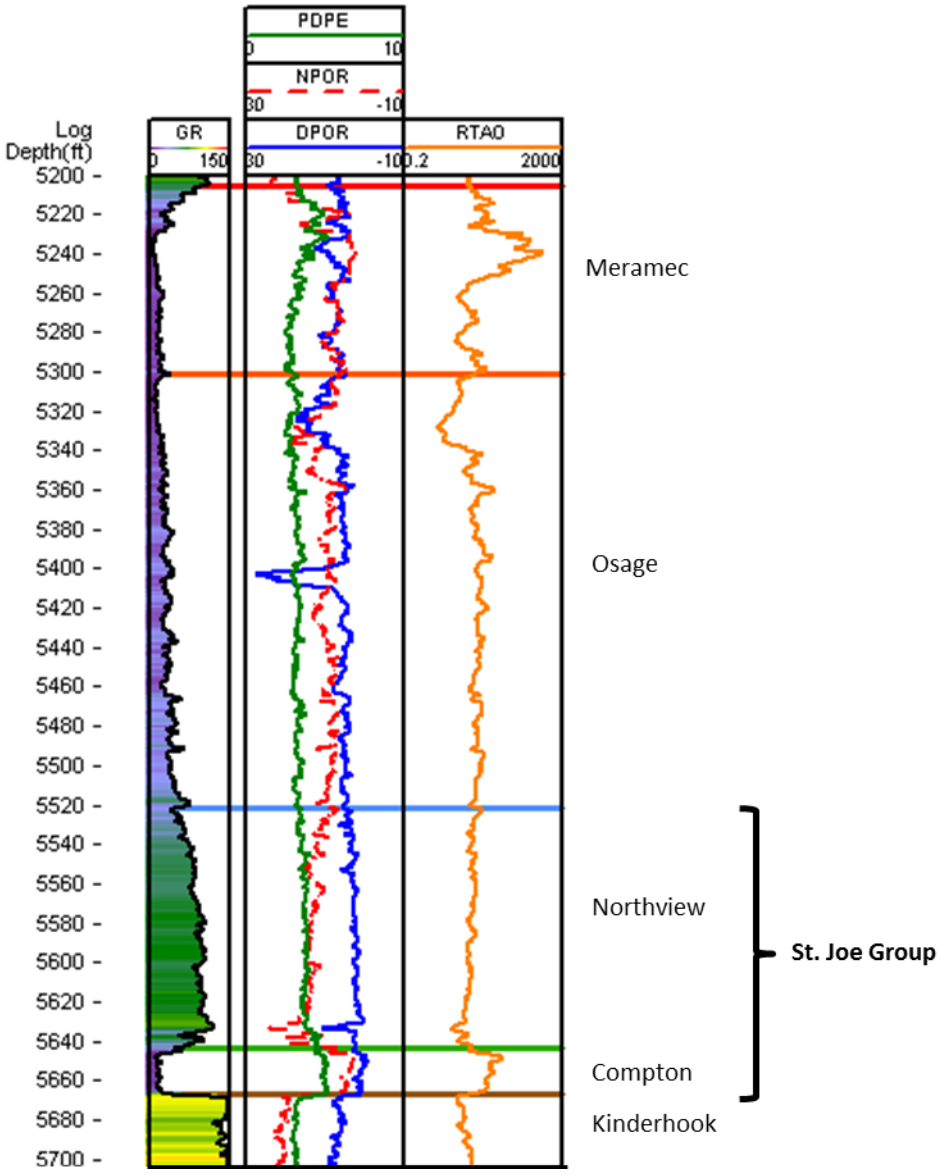

Figure 7 Log curves through the Mississippian series for the Scribner #1 SWD. GR = gamma ray, PDPE = photo electric effect, NPOR = neutron porosity, DPOR = density porosity, RTAO = deep resistivity

2.3.1 Kinderhookian

The Kinderhook Formation overlies the Devonian Woodford Shale and marks the base of the Mississippian System. The Kinderhook Formation is easily differentiated from the Woodford Shale which has higher gamma ray API units ranging from 200 to 400 (Figures 6 and 7). The Kinderhook Formation has gamma ray readings in the range of 75 to 190 units. The the mudlogs on the Reitz #2 SWD report the Kinderhook Formation consisits of dark to grey shale, with silty to gritty texture, and trace pyrite.

The St. Joe Group is Kinderhookian in age and overlies the Kinderhook Shale. Only the Compton and Northview Formation are present in the study area (Figure 5). The Compton Formation has a photo-electric effect measurement between 4 and 5 barnes/electron, which indicates that it is a fairly clean limestone with little or no chert. In the study area, the Compton Formation thickness ranges from 10 to 25 ft. According to Manger and Evans (2012), the Compton Formation in outcrop consists of crinozoan packstones and wackstones with minor occurrences of chert.

The Northview Formation, overlying the Compton Formation, is a thin light green to grey calcareous shale (Cahill 2012). The photo-electric effect log measurements average around 3 barnes/electron with a characteristic neutron/density shale crossover effect. Gamma ray readings range from 30 to 120 API units. The logs used in this study suggest that the Northview shale grades into the Osage Formation.

2.3.2 Osagean

The Oasagean series is a chronostratigraphic interval characterized by an overall increase in silica content. The Osage Formation is a cherty limestone with varying amounts of silica. The photo-electric effect measurement was used to interpret intervals

of higher or lower silica content. The Osage Formation is differentiated into a Lower Boone and Upper Boone members based on silica content (Cahill 2012). According to Manger and Evans (2012), the Lower Boone member is a calcisiltite with penecontempoaneous chert development, while the Upper Boone member consists of crinozoan detritus that experienced later diagenetic chert replacement.

2.3.3 Meramecian

The Mereamecian series includes Meramec Formation that unconformably overlies the Osage Formation. The transition from Osage to Meramec is usually represented by a decrease in chert content in the Meramec Formation, which is a dolomitic crinoidal wackestone and packestone with less chert (Thornton, 1964; Costello et al., 2013).

Chapter 3

Previous Work

At this time there is no standardized definition or measurement of brittleness (Yang et al., 2013). According to Jin et al., (2014), more than twenty expressions for brittleness are found in literature. These expressions range from mineralogical inputs to mechanical property inputs and may be measured in the field, laboratory, or in the subsurface using well log measurements. The expressions referenced in the thesis are in table 1.

Rickman's (2008), definition of brittleness (B_1 of Table 1) is estimated directly from Young's Modulus and Poisson's Ratio where high values of Young's Modulus (E) and low values of Poisson's ratio (ν) are indicators for brittleness. The equation used by Rickman takes the values of static Young's Modulus and Poisson's Ratio derived from Mullen's et al., (2007) composite method, then averages them and calculates a percentage. When the brittleness curve is generated, a cutoff value is determined in a ductile clay-rich shale so the higher the values above the cutoff, the more brittle the rock.

Sharma and Chopra (2012) proposed a seismic attribute definition of brittleness (B_2 Table 1) using the product of Young's Modulus and density to detect changes in brittleness. A rock with high Eρ would be more brittle than one with a low value.

The Goodway et al. (2007) definition (B_3 Table 1) is more useful with seismic data. It converts E and ν to Lame's parameters of incompressibility and rigidity, Lambda (λ) and Mu (μ) respectively. Low incompressibility (λ) and high rigidity (μ) is used to determine the more brittle zones.

Jin et al., (2014) compared brittleness curves generated from internal friction angles (B_4 Table 1), Young's Modulus and Poisson's Ratio (modified from Rickman's brittleness equation) (B_1 Table 1), and mineralogical brittleness (B_5 Table 1). All curves

had similar shapes with different magnitudes in various shale plays (Figure 8). They found that the current definitions of brittleness are not sufficient to be used independently as indicators of fracability in shale reservoirs. They used a new mineralogical definition of brittleness (B_5 Table 1) along with fracture toughness to determine a fracability index. For their work, fracture toughness was determined from correlations of fracture toughness with Young's modulus as follows:

$$K_{IC} = 0.313+0.027x$$

Where x= Young's Modulus in GPa

Jennings (2012) also compared various definitions of brittleness in the Mississippian limestone of Osage County, Oklahoma. Jennings's used definitions of brittleness outlined by Rickman (2008) (B_6 Table 1), Goodway (2007) (B_3 Table 1), and Sharma and Chopra (2012) (B_2 Table 1). The purpose of Jennings's work was to segregate the Mississippian section into discernable and potentially correlatable units based on brittleness (Figure 9). According to Jennings, the three definitions gave similar results.

Table 1 Brittleness expressions referenced in this thesis

Brittleness Equation	Variable Description	Test Method	Reference
$B_1 = (E_n+\nu_n)/2$	E_n and ν_n are normalized (dynamic) Young's Modulus and Poisson's Ratio, respectively	Sonic and density logging	Jin et al., 2014
$B_2 = E\rho$	E is Young's Modulus and ρ is density	Sonic and density logging	Sharma and Chopra, 2012
$B3 = \lambda/(\lambda+2\mu)$	λ is Lame's Parameters and μ is Shear Modulus	Sonic and density logging	Goodway et al., 2007
$B_4 = \sin\phi$	ϕ is the internal friction angle	Mohr circle or logging data	Hucka and Das, 1974
$B_5 = (W_{QFM}+W_{carb})/W_{total}$	W_{QFM} is the weight fraction of quartz, feldspar, and mica. W_{carb} is the weight fraction of dolomite, calcite, and other carbonate minerals. W_{total} is the total mineral weight	Mineralogical logging or XRD	Jin et al., 2014
$B_6 = (E\_C + \nu\_C)/2$	E_C and ν_C are normalized (static) Young's Modulus and Poisson's Ratio, respectively	Composite Mechanical Rock Property Model (CMRPM)	Rickman et al., 2008 Mullen et al., 2007
$B_7=F_d=(\mu(A(\nu/(1-2\nu))+B))/U_a$	F_d is fracture density. μ is Shear Modulus. And B are expressed in terms of the strain invariants, where $A=I_1^2$ and $B=I_1^2-2I_2$. ν is Poisson's Ratio, and U_a is energy per fracture area created	Sonic and density logging.	Wickham et al., 2013

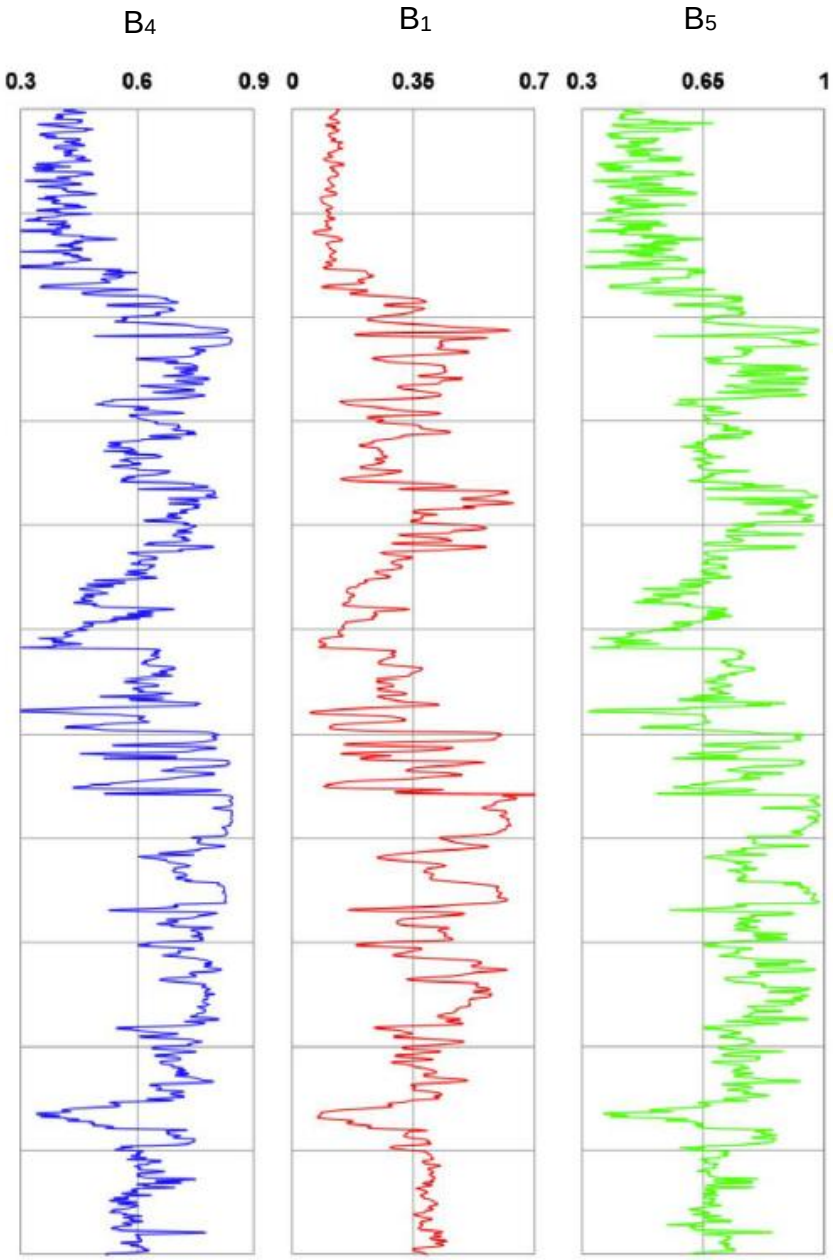

Figure 8 Comparison of curves generated from definitions of brittleness (Jin et al., 2014) (B_4, B_1 and B_6 from Table 1)

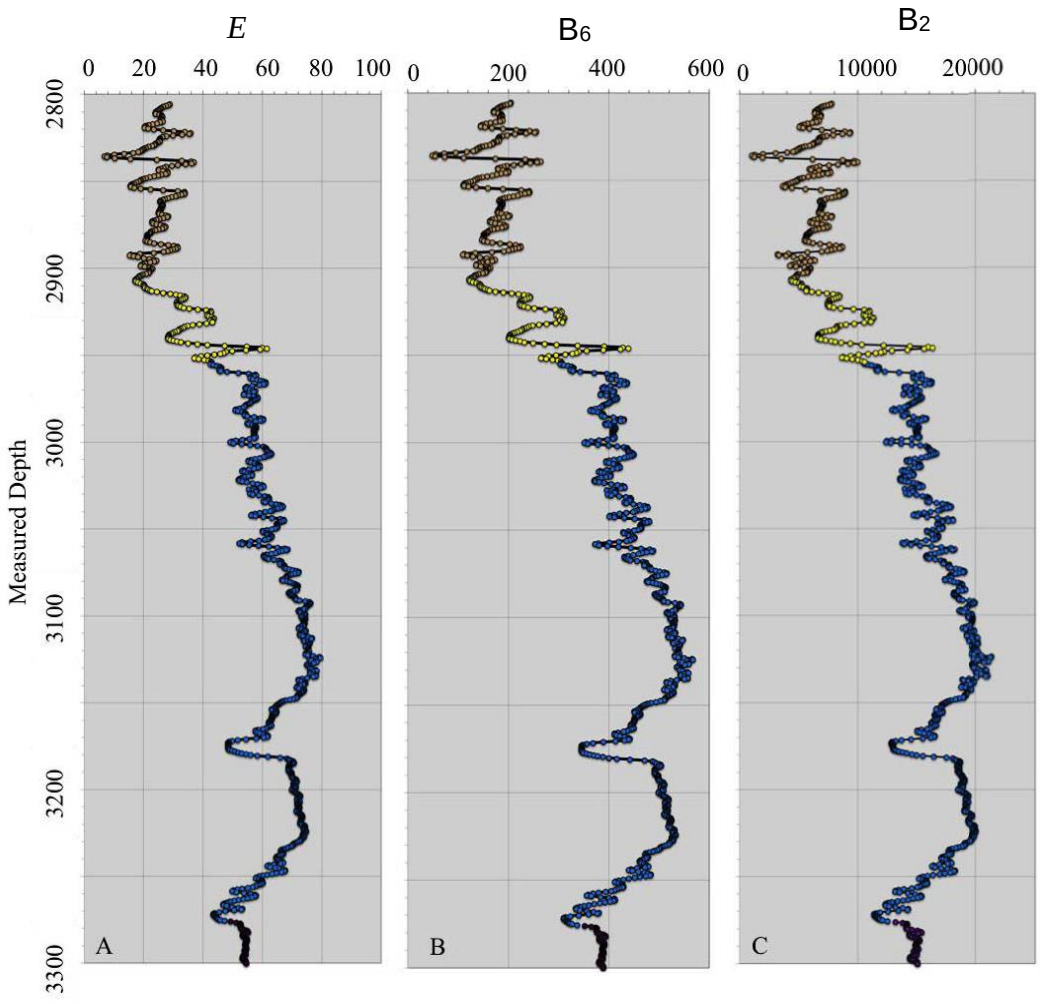

Figure 9 Comparison of curves generated from definitions of brittleness (Jennings 2012) (B_6 and B_2 from Table 1; *E* is Young's Modulus)

Chapter 4

Derivation of Brittleness Equation

In this study, a brittleness log was be created using a new expression for brittleness based on fracture density proposed by Wickham et al., (2013). The resulting log was compared to logs produced by other brittleness definitions. The expected result is that this new log will provide a better method for identifying brittle zones based on fracture density.

Table 2 Symbols used

Symbol	Meaning
U_v	Strain energy in volume
G_C	Critical energy release rate
σ	Stress
ε	Strain
F_d	Fracture density
U_a	Energy per fracture area created
μ	Elastic Shear Modulus
E	Young's Modulus
ν	Poisson's Ratio
V_P	Compressional wave velocity
V_S	Shear wave velocity
I_1	First strain invariant
I_2	Second strain invariant
K_{IC}	Critical stress intensity factor for Mode I fractures

The new equation is based on an energy relationship published by Sih (1985). According to Sih, “the surface and volume energy density of each material element are related by the rate of change of volume with surface.”

This is expressed as a Differential Equation:

$$(\frac{dA}{dV})_i\,(\frac{dU}{dA})_i = (\frac{dU}{dV}) \quad \text{(Eq. 1)}$$

Where A is fracture surface area, V is volume and U is ~~strain~~ energy. For the purpose of this study the integrated form over a volume element is used:

$$(F_d)(U_a) = U_v \quad \text{(Eq. 2)}$$

Where F_d is the fracture density (fracture surface/volume); U_a is the energy needed to create fracture area A (related to surface energy density); and U_v is the strain energy density.

Strain energy density, U_v, is expressed in the general case as:

$$U_v = \frac{1}{2}(\sigma_{xx}\varepsilon_{xx} + \sigma_{yy}\varepsilon_{yy} + \sigma_{zz}\varepsilon_{zz}) + (\sigma_{xy}\varepsilon_{xy} + \sigma_{yz}\varepsilon_{yz} + \sigma_{xz}\varepsilon_{xz}) \quad \text{(Eq. 3)}$$

Using Hooke's Law and substituting, a new equation is derived which expresses strain energy density in terms of strain, Poisson's Ratio, and Shear Modulus. Assuming elasticity, the strain energy density in a particular rock volume of constant elastic properties is:

$$U_v = \frac{\nu\mu}{1-2\nu}(\varepsilon_{xx} + \varepsilon_{yy} + \varepsilon_{zz})^2 + \mu(\varepsilon^2_{xx} + \varepsilon^2_{yy} + \varepsilon^2_{zz}) + 2\mu(\varepsilon^2_{xy} + \varepsilon^2_{yz} + \varepsilon^2_{xz}) \quad \text{(Eq. 4)}$$

Where v= Poisson's Ratio, μ = Shear Modulus and U_v is the total elastic strain energy, some of which can be used to create fracture surface area.

For coordinates parallel to the principal direction of strain, Eq. 4 becomes:

$$U_v = \frac{\nu\mu}{1-2\nu}(\varepsilon_1 + \varepsilon_2 + \varepsilon_3)^2 + \mu(\varepsilon^2_1 + \varepsilon^2_2 + \varepsilon^2_3) \quad \text{(Eq. 4B)}$$

Using the strain invariants Eq. 4B is simplified into Eq. 5:

$$U_v = \mu(A(\frac{\nu}{1-2\nu}) + B) \quad \text{(Eq. 5)}$$

where:

$$A = I_1^2 \text{ , and}$$

$$B = I_1^2 - 2I_2$$

The strain invariants are:

$$I_1 = \varepsilon_1 + \varepsilon_2 + \varepsilon_3$$

$$I_2 = \varepsilon_1\varepsilon_2 + \varepsilon_2\varepsilon_3 + \varepsilon_3\varepsilon_1$$

Substituting the strain invariants into the equations for A and B, then simplifying:

$$A = I_1^2 = (\varepsilon_1 + \varepsilon_2 + \varepsilon_3)^2 = \varepsilon^2_1 + \varepsilon^2_2 + \varepsilon^2_3 + 2(\varepsilon_1\varepsilon_2 + \varepsilon_2\varepsilon_3 + \varepsilon_3\varepsilon_1)$$

$$B = I_1^2 - 2I_2 = \varepsilon^2_1 + \varepsilon^2_2 + \varepsilon^2_3 + 2(\varepsilon_1\varepsilon_2 + \varepsilon_2\varepsilon_3 + \varepsilon_3\varepsilon_1) - 2(\varepsilon_1\varepsilon_2 + \varepsilon_2\varepsilon_3 + \varepsilon_3\varepsilon_1) = \varepsilon^2_1 + \varepsilon^2_2 + \varepsilon^2_3$$

Substituting Eq. 5 into Eq. 2 then solving for F_d gives:

$$F_d=\frac{\mu(A(\frac{v}{1-2v})+B)}{Ua} \quad \text{(Eq. 6)}$$

Energy per Fracture Area U_a, is related to the Critical Energy Release Rate G_C:

$$U_a=\frac{G_C}{2} \quad \text{(Eq. 7)}$$

Mode I fracture toughness, K_{IC}, is related to critical energy release rate, G_C by Equation 8 (Irwin, 1958):

$$G_C=\frac{K_{IC}^2}{E} \quad \text{(Eq. 8)}$$

By combining equations 7 and 8, then substituting into equation 6, the equation we are using to create the brittleness log is:

$$F_d=\frac{(A\left(\frac{v}{1-2v}\right)+B)(4\mu^2(1+v))}{K_{IC}^2} \quad \text{(Eq. 9)}$$

Where E was rewritten as $2\mu(1+v)$.

For this study, dynamic elastic properties were derived from P-wave and S-wave velocities from dipole sonic logs and densities from density logs collected from vertical wells drilled through the Mississippian Section in the study area. Measurements from log data gathered from the subsurface reflect the insitu conditions of the formation.

Chapter 5

Methodology

5.1 Data Acquisition

Acoustic, density, porosity and microresistivity image logs were acquired from two vertical disposal wells (Scribner #1 SWD in Woods county and Reitz #1 and #2 in Alfalfa county) drilled through the Mississippian sequence in northern Oklahoma. For the Scribner #1 SWD well, dipole sonic, density, porosity, resistivity and micro-resisitivity image logs were run by Halliburton. The data was provided in two forms: A display format with generated curves (Figure 5-1) and the digital data in the form of an LAS file. Weatherford's microresistivity image log run on the Reitz #1 was used as a proxy for the Reitz #2, which was drilled aprroximately 150 feet away (Figure 1). Weatherford's dipole sonic and density logs were run on the Reitz #2. There was approximately 450 feet logged through the Mississippian section from each well. The sample rate of the logging tools was every half foot, giving around 900 data points per well. The image log data was interpreted for natural fractures by Sherif Gowelly, formerly of Fronterra Geosciences and currently working as lead interpreter for Weatherford.

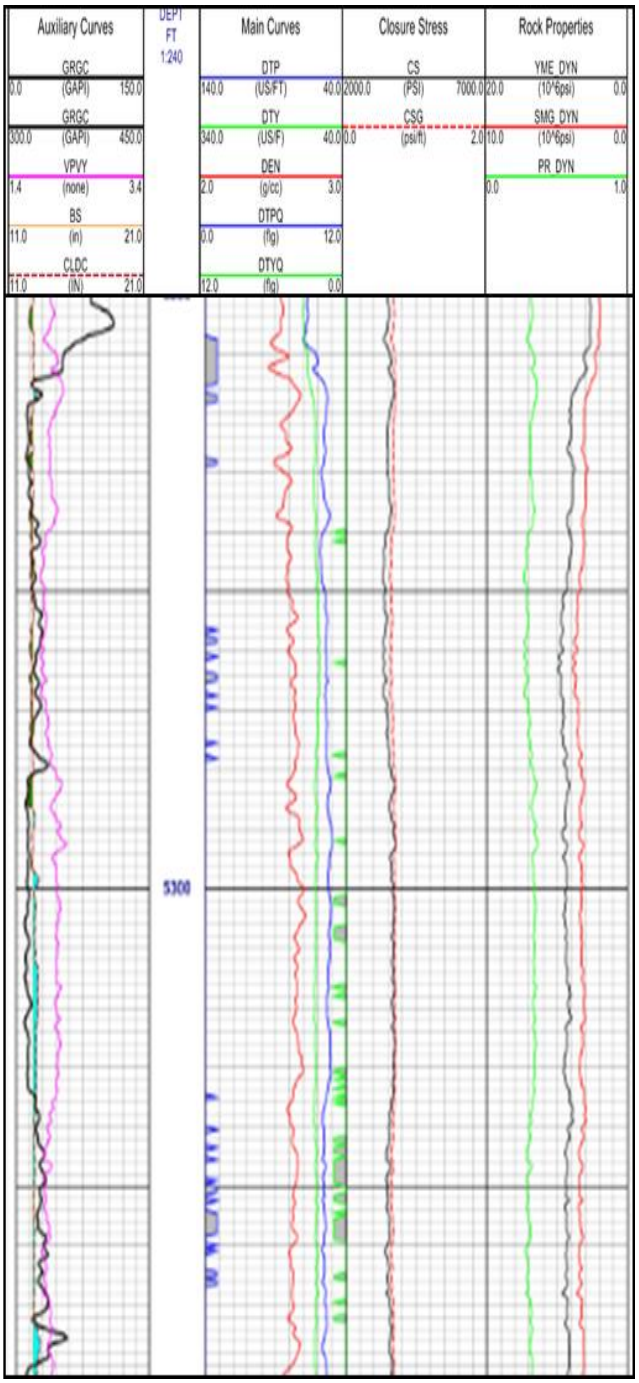

GRGC	Gamma Ray
VPVY	VP/VY Ratio
BS	Bit size
CLDC	Density Caliper
DTP	Compressional Delta T
DTY	YY Dipole Shear Delta T
DEN	Compensated Density
DTPQ	DTP Semblance Quality Flag
DTYQ	DTY Semblance Quality Flag
CS	Closure Stress
CSG	Closure Stress Gradient
YME_DYN	Young's Modulus (Dynamic)
SMG_DYN	Shear Modulus (Dynamic)
PR_DYN	Poisson Ratio (Dynamic)

Figure 10 Sample of the displayed version of the dipole sonic log provided by Weatherford on the Reitz #2 SWD covering the Upper Mississippian

5.2 Raw Data Conversions

Raw data from dipole sonic logs and density logs from 2 vertical wells drilled in the study area were recorded in imperial units, μs/ft and g/cm^3 respectively. Where Delta T (μs/ft), is a measure of sonic slowness and must be converted to velocity (m/s). Once the appropriate conversions to SI units were made, dynamic elastic parameters could be calculated at every half foot coinciding with the log measurements using the following equations:

Shear Modulus (Pa)

$$\mu = V_S^2 \rho$$

Young's Modulus (Pa)

$$E = \frac{\rho V_S^2 (3V_P^2 - 4V_S^2)}{V_P^2 - V_S^2}$$

Poisson's Ratio

$$\nu = \frac{.5(V_P^2 - 2V_S^2)}{V_P^2 - V_S^2}$$

5.3 Fracture Toughness

Fracture toughness is a fundamental parameter in fracture mechanics, describing resistance of a material to crack propagation (Chang et al., 2001). Although a more precise measurement of fracture toughness can be achieved with core samples in a lab, these methods are impractical and not economically viable in most wells. For this study, empirical relationships between fracture toughness and Young's Modulus were used to estimate fracture toughness. Whitaker et al. (1992) compiled measurements of fracture

toughness and elastic properties on a variety of rock types that were used to make correlations between fracture toughness and elastic propertiesas well as sonic velocities. A best fit line was generated so that the correlation equation could be used to estimate fracture toughness based on Young's Modulus data from the logs. For this study, correlation equations for limestone, siltstone, shale, and dolomite were used (Figures 11,12,13,14). Due to the heterogeneity of the lithology within the Mississippian section, an estimate of lithology was determined from neutron density crossplots and gamma ray readings to generate a weighted fracture toughness correlation equation at each measured point of the log. For example, each intercept and slope of each lithology correlation equation was multiplied by its estimated percent volume of rock. Then, the calculated slopes and estimated intercepts for each lithology were added together to estimate a new slope and intercept to be used in the fracture toughness correlation equation for the measured depth (Table 3).

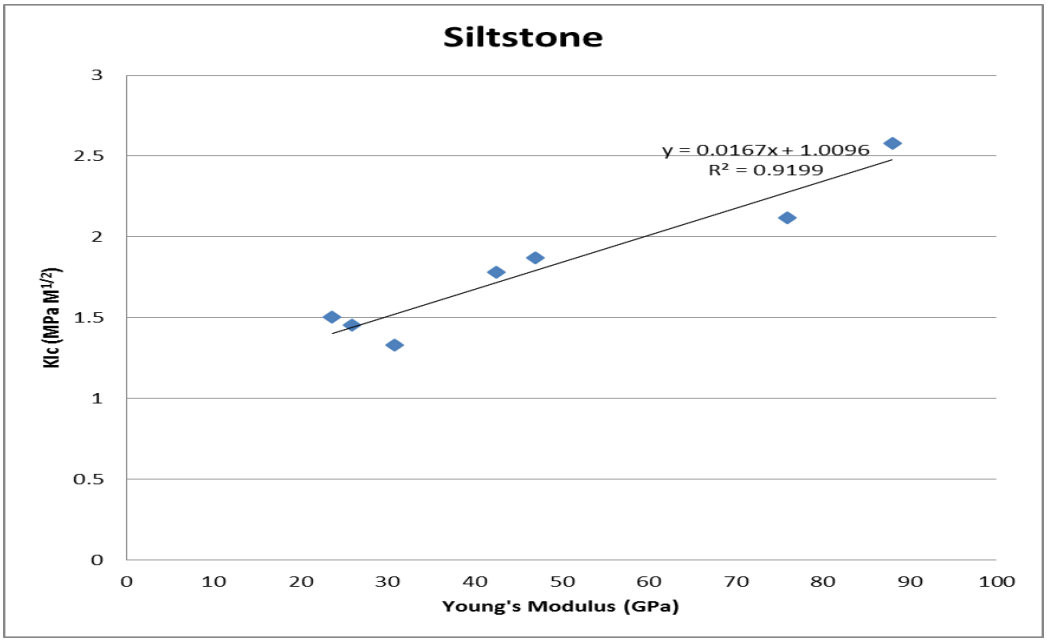

Figure 11 Plot of Young's Modulus and fracture toughness from laboratory data collected on siltstones (Whitaker et al., 1992)

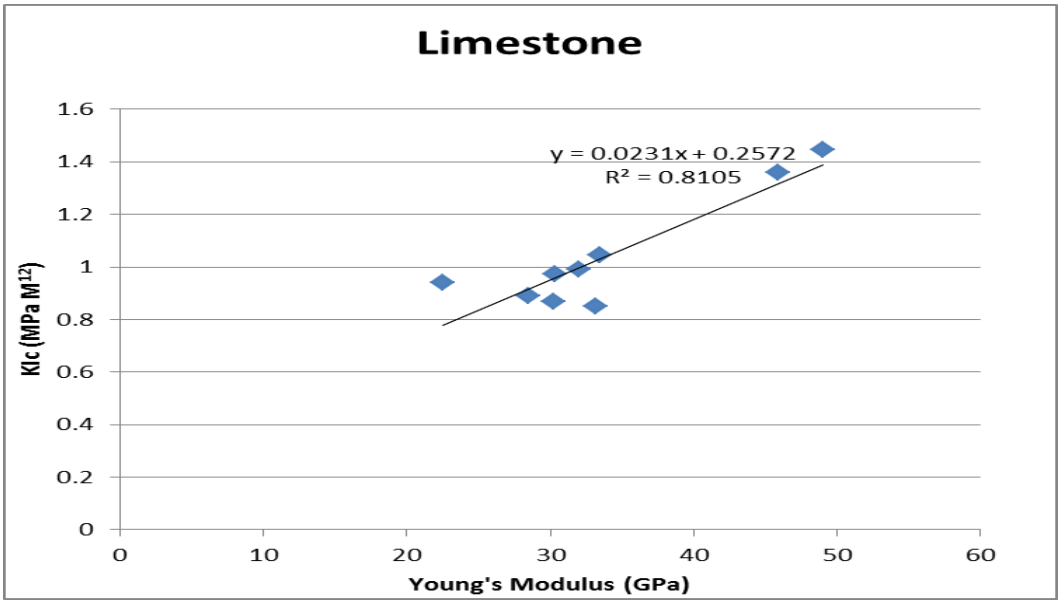

Figure 12 Plot of Young's Modulus and fracture toughness from laboratory data collected on limestone (Whitaker et al., 1992)

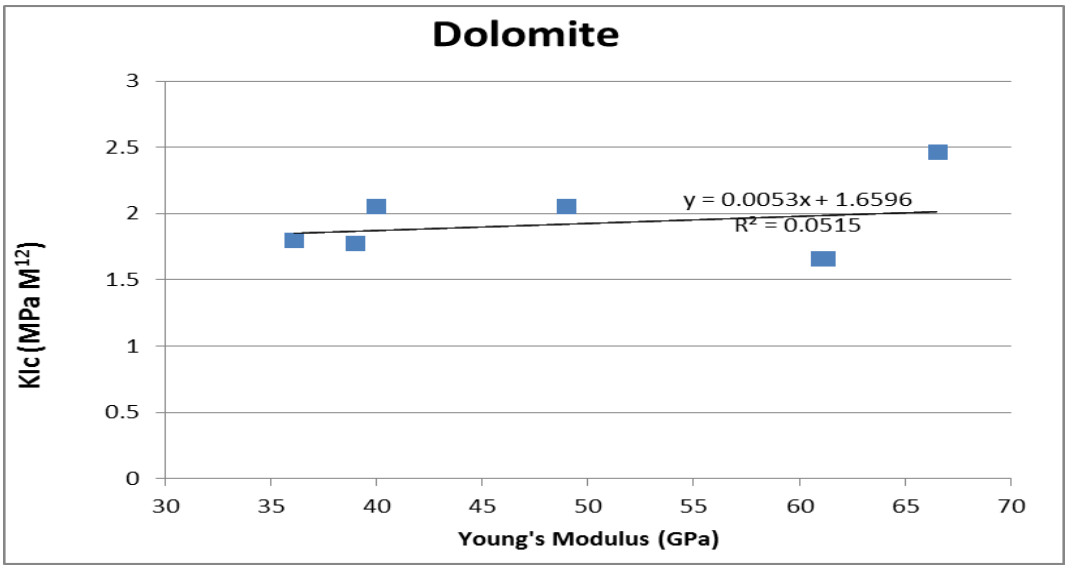

Figure 13 Plot of Young's Modulus and fracture toughness from laboratory data collected on dolomites (Whitaker et al., 1992)

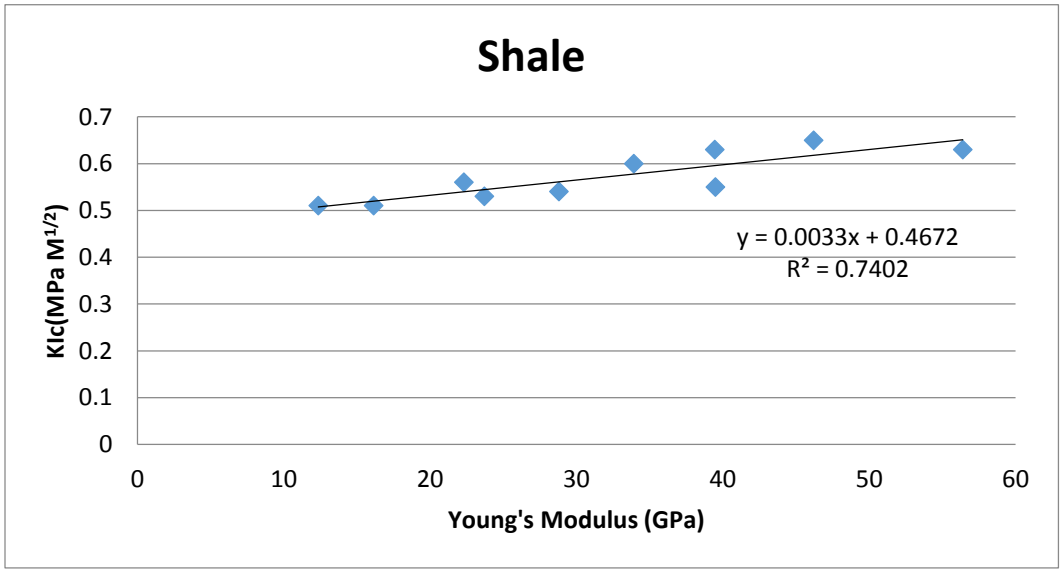

Figure 14 Plot of Young's Modulus and fracture toughness from laboratory data collected on shale (Whitaker et al., 1992)

Table 3 Example showing the lithology weighted slopes and intercepts calculated for use in the fracture toughness equation

Lithology	Slope	Intercept	Rock type proportion	New Slope	New Intercept
Limestone	0.023	0.257	0.88	0.02024	0.22616
Siltstone	0.0167	1.0096	0.07	0.001169	0.070672
Clay/shale	0.0033	0.467	0.04	0.000132	0.01868
Dolostone	0.0053	1.66	0.01	0.000053	0.0166
Sandstone	0.027	0.166	0	0	0
Sum				0.021594	0.332112

5.4 Image Log Interpretation

With the exception of core analysis, acoustic or micro-resistivity image logs provide the best opportunity to detect fractures in a wellbore. Micro-resistivity image logs were run on each of the wells used for this study. An expert interpretation was done by Sherif Gowelly, the lead image log interpreter for Weatherfod International. His work provided a quantitative analysis of observed natural fractures from the micro-resistivity log. His natural fracture plot was used to compare to the results of the brittleness log created from this study. His interpretation was reviewed to make sure all the fractures were present and were natural.

Interpreting natural fractures from image logs can be challenging. Drilling induced fractures usually strike parallel to the maximum horizontal stress direction, h_{max} (Figure 5-6). Borehole breakouts occur parallel to the minimum stress direction, h_{min} (Figure 5-6). Natural fractures in image logs may exhibit different geometries. If the

natural fracture cuts across the wellbore, then the fracture will apear as a full sinewave in the image log. Some natural fractures may appear as partial sinewaves if they terminate against a bedding surface, or against another fracture (Figure 5-7).

Identification of natural fractures from image logs may depend on the interpreter doing the work. The interpretation is subject to the quality of the tool measurement and the quality of the resulting processed image used for interpretation.

There is another issue with using natural fractures interpreted from image logs to correlate with the proposed brittleness curves. The wellbore acts a a scanline and depending on the angle of the fractures to the wellbore the fracture density observed may be significantly biased (Chiles et al., 2008). In the case of this study most of the fractures dip greater than 65 degrees whereas the wellbore is vertical. The high angle of the fractures do not allow an unbiased estimate of the fractures present.

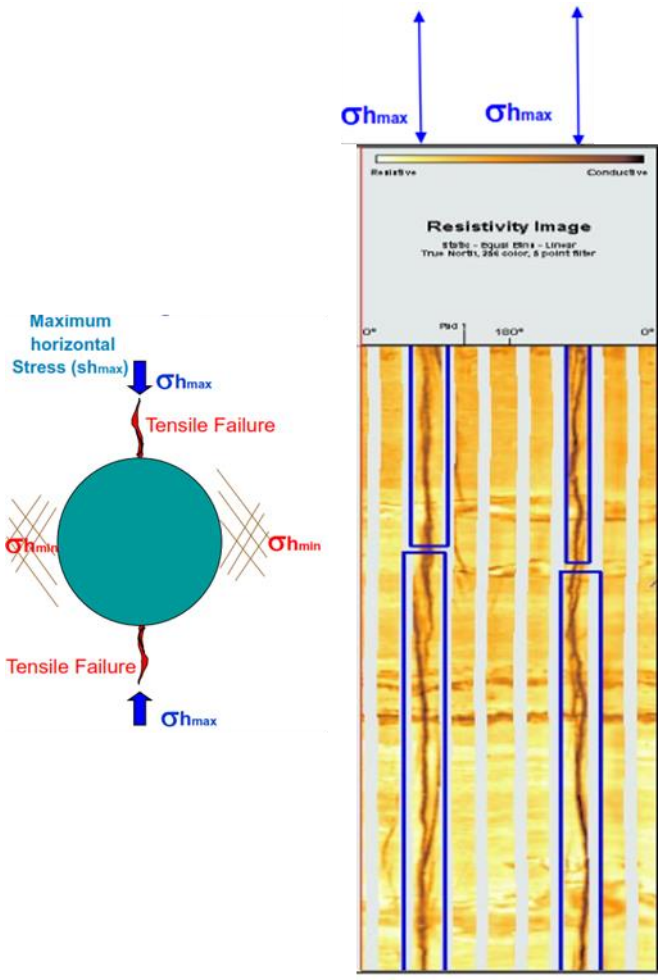

Figure 15 Illustration showing identification of drilling induced fractures as seen in a vertical wellbore from a microresistivity log (Modified from Fronterra Geosciences)

- Fractures that intersect the entire wellbore show a complete sinewave

- Illustrated at right are
  - **Full sinewave** fractures with **no shear**; i.e. no offset of bedding or other fractures (**Pale Blue**)
  - **Full sinewave** fractures with **apparent shear**; i.e. that **offset** bedding and/or pre-existing fractures (**Red**)
- Some fractures however, show only:
  - **Partial sinewaves** (**Yellow**)
- These partial fractures can show a variety of **termination types**
  - **Type 1** terminates against bedding surfaces
  - **Type 2** terminates against other fractures
  - **Type 3** terminates against a shear fracture (i.e. offset by, & therefore predates, the shear fracture)
  - **Type 4** terminates within a particular bed, but not against any obvious or visible surface

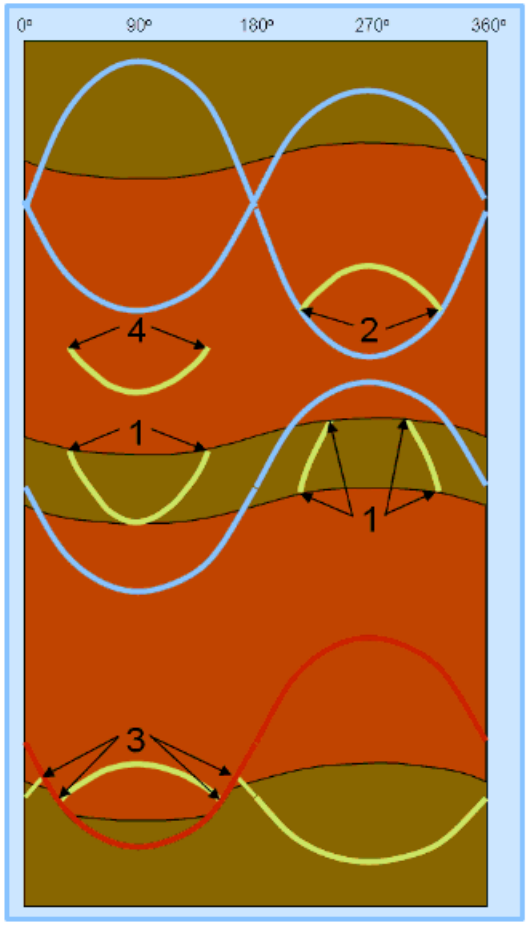

Figure 16 Explanation of fracture identification from image logs (Fronterra Geosciences)

5.5 Workflow

Due to the heterogeneity of the Mississippian Series in the study area an estimate of the percentage of shale, limestone, dolomite, and sandstone was made by generating lithology crossplots using the petrophysical log analysis software HDS. Volume of shale was determined from gamma ray using a minimum reading of 10 API units and a maximum reading of 140 API units. The percentages of lime, sand, and dolomite were estimated from a neutron-density crossplot for both the Reitz #2 SWD well (Figure 5-8) and the Scribner #2 SWD well (Figure 5-9). Based on the lithology percentages, a weighted correlation equation for fracture toughness and Young's Modulus was calculated and used to determine the fracture toughness for each log data point.

Once the log measurements were converted to SI units, the inputs for the new brittleness curve were calculated. The data was loaded into Petra to generate the new brittleness curve.

Fracture frequency was interpreted from micro-resistivity image logs by Sherif Gowelly. The fracture identification interpretations were reviewed and verified. The frequency of natural fractures determined from the image logs was used to compare with the resulting brittleness log. Curves were also generated in Petra using Jin's (2014) and Sharma and Chopra's (2012) definitions of brittleness to compare to the new brittleness curve.

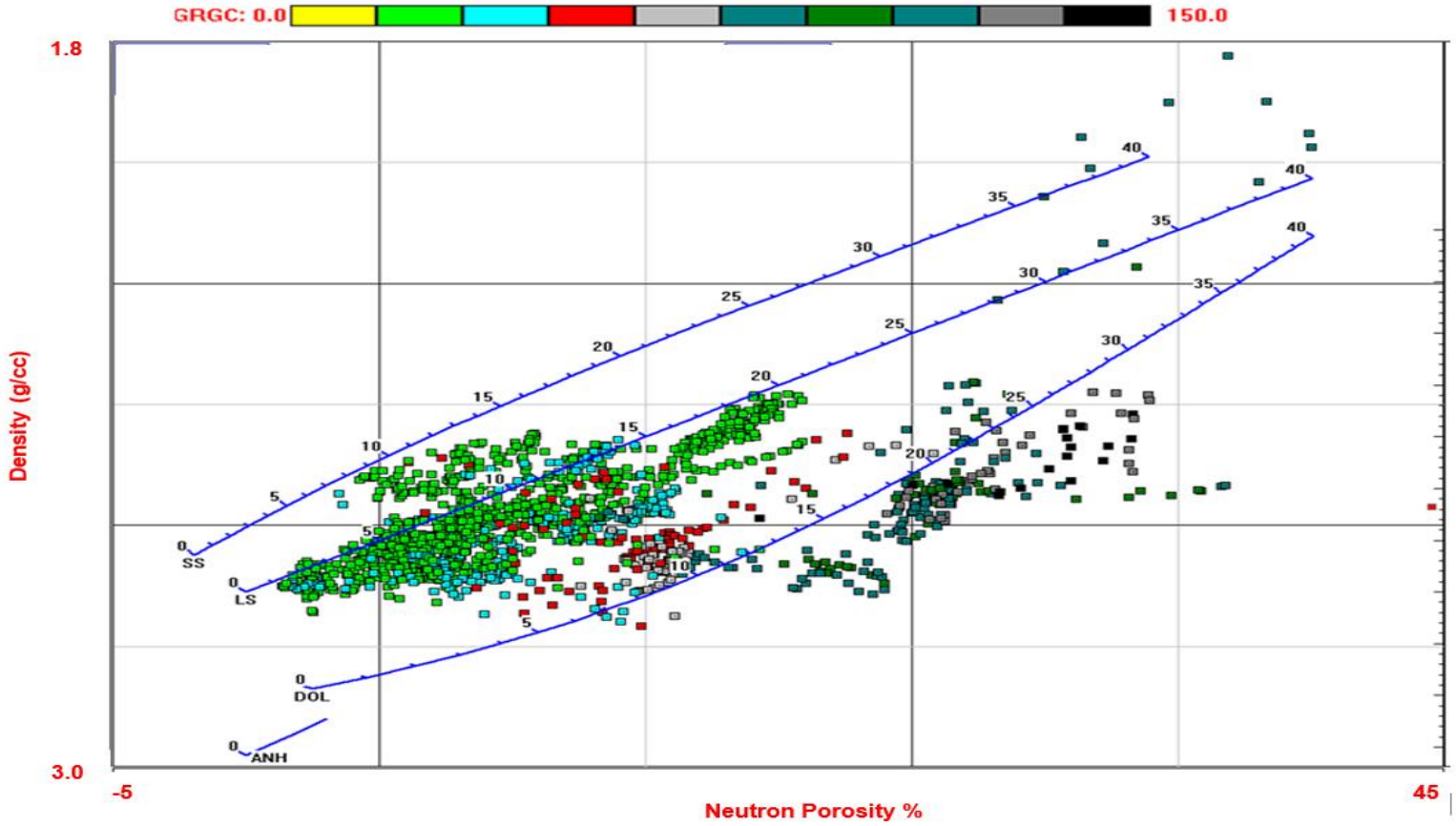

Figure 17 Lithological distribution in the Reitz #2 SWD, estimated from a neutron-density crossplot. Color scale of data points corresponds with gamma ray readings (GRGC). Values lying along the blue lithology lines reflect corrected porosity for that lithology. (SS = sandstone; LS = limestone; DOL = dolomite; ANH = anhydrite)

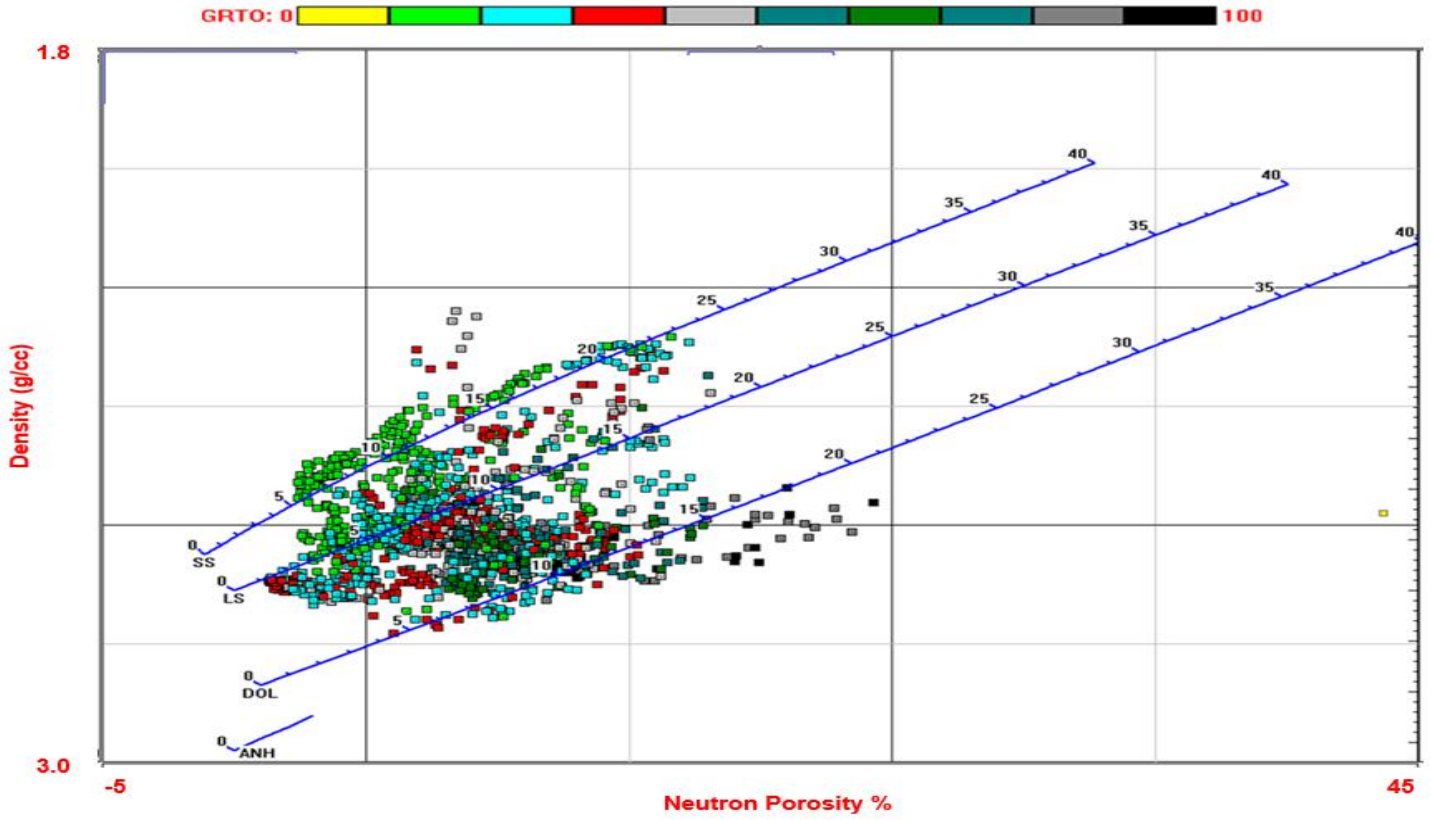

Figure 18 Lithological distribution in the Scribner #1 SWD, estimated from a neutron-density crossplot. Color scale of data points corresponds with gamma ray readings (GRGC). Values lying along the blue lithology line indicators reflect corrected porosity for that lithology. (SS = sandstone; LS = limestone; DOL = dolomite; ANH = anhydrite)

Chapter 6

Results and Discussion

The new fracture density or brittleness curve (B_7 Table 1) is based on geomechanical principles and incorporates all the dynamic linear elastic parameters as well as fracture toughness. Various ways of analyzing the new curve's effectiveness in determining brittle layers included 1) comparisons with Jin's et al., (2014) and Sharma and Chopra's (2012) definitions of brittleness, equations B_1 and B_2 (Table 1), respectively, and 2) comparisons with natural fracture abundance or intensity from image logs.

6.1 Reitz #2 SWD

Figure 19 illustrates plots of the different curves for this well based on the various definitions of brittleness selected for comparison in this study. Each curve is displayed as a percentage. A plot of the interpreted natural fractures from the image log on the Reitz #1 SWD, was used because Reitz #2 SWD had no image log and Reitz #1 SWD was only 150 feet away so correlation was not a problem.

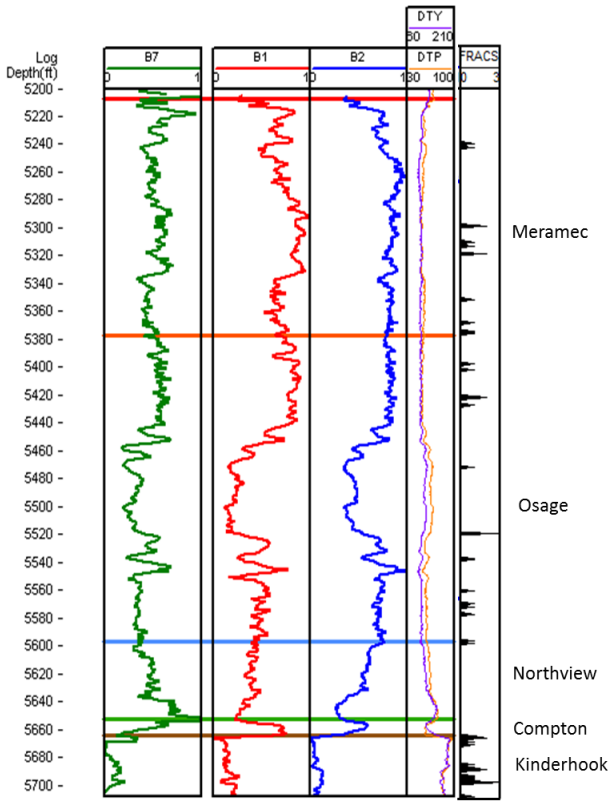

Figure 19 Comparison between the new brittleness curve, B_7, Jin's et al., (2014) B_1, Sharma and Chopra's (2012) B_2 and a plot of the natural fractures derived from the image log interpretation from nearby Reitz #2 SWD. DTP = Delta T Compressional; DTY = Delta T Shear

Like Jennings's (2012) findings, variations observed in each of the logs' character are slight and vary mostly in scale, with the exception of the Northview Formation. From the top of the Northview Formation to the top of the Compton Formation, all three curves have different indications of brittleness. The new curve (B_7 Table 1) indicates an increase in brittleness as the section is traversed downward. Jin's et al., (2014) curve, (B_1 Table 1), shows little change in brittleness through the interval

and little change in brittleness from the interval above. The curve, B_2, shows an opposite response to what B_7 indicated. According to Sharma and Chopra's definition (B_2 Table 1), this interval tends to become much less brittle in the lower part of the formation. The interpreted fracture plot revealed some fracturing at the top of this interval but no fracturing in the Northview Formation.

The curves for all three had similar indicators of brittleness through the Compton Formation. Each curve suggests the Compton is brittle and in both B_1 and B_2, there is a clear delineation of brittleness between the overlying and underlying formations. No fracturing was interpreted from the image logs over this interval despite all three curves showing that this formation was brittle.

In each case, the Kinderhook Formation is the least brittle in the Mississippian section. This conclusion seems reasonable based on the high clay content of the Kinderhook Formation. However, the interpretation of the image logs shows that the Kinderhook is highly fractured.

6.2 Scribner #1 SWD

Data from the Scribner #1 SWD were used to compare the same brittleness definitions applied to the Reitz #2 SWD. The interpreted natural fractures derived from the image log were used to test the brittleness curves.

Overall, the brittleness curve (B_7 Table 1), has a very similar shape to the curve generated from Sharma and Chopra's (2012) definition of brittleness. The curve generated from Jin's (2014) definition of brittleness (B_1 Table 1) shows brittleness shifts on a much smaller scale. B_1, suggests that there is little brittleness change within the Mississippian section outside of the Compton Formation. Both B_7 and B_2, have very

similar log curve character, with the exception of the Compton and Kinderhook Formations.

The Compton and Kinderhook Formations have significant changes in the mechanical properties of the rock affecting brittleness. In the Compton Formation, B_2 and B_1 indicate much higher brittleness than the overlying Northview Formation while B_7 shows about the same brittleness as the Northview Formation. The brittleness prediction in the Kinderhook Formation is the most puzzling. Both B_1 and B_2 indicate that the brittleness of the Kinderhook Formation is much lower than the Compton Formation. However, B_7, shifts to a much higher brittleness in the Kinderhook Formation. This was a complete opposite response to that seen in B_1 and B_2. From the estimated lithologies from the crossplots there was a lithology variation within the Kinderhook between the Reitz #2 and Scribner #1 SWD wells. In the Reitz #2 SWD well, there was a more mixed lithology estimated in the Kinderhook Formation than the Scribner #1 SWD where the estimated lithology was almost completely shale.

From the natural fracture plot derived from the image log there are fewer natural fractures in the Scribner #1 SWD well than the Reitz #1 SWD. There does not seem to be a clear correlation between the interpreted natural fractures and the brittleness curves generated from this study. For example, near the top of the Mississippian section, both B_7 and B_2 brittleness curves indicate low relative brittleness yet many fractures were observed from the image log

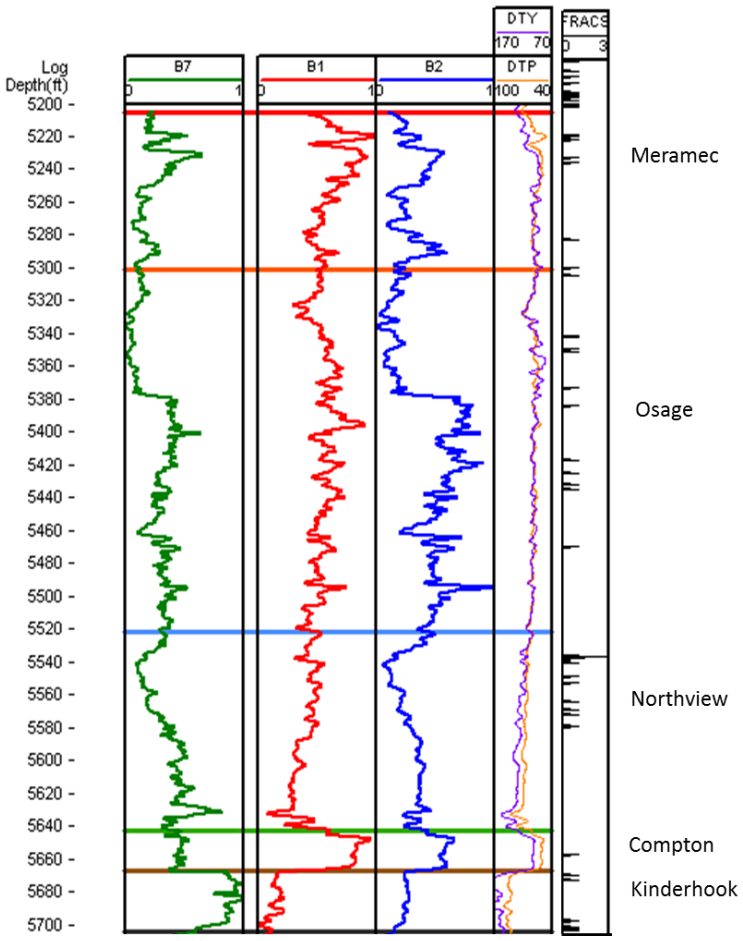

Figure 20 Comparison between the new brittleness curve, B_7, Jin's et al., (2014) B_1, Sharma and Chopra's (2012) B_2 and a plot of the natural fractures derived from the image log interpretation. DTP = Delta T Compressional; DTY = Delta T Shear (Scribner #1 SWD)

6.3 Discussion

The purpose of this work is to compare a new geomechanical brittleness definition with other definitions of brittleness by Jin et al., (2014) (B_1 Table 1) and Sharma and Chopra (2012) (B_2 Table 1). For each well, the three brittleness definitions predict significant

changes in brittleness throughout the Mississippian section. The new geomechanical definition (B_7 Table 1) predicted clear divisions of brittle and non-brittle zones. However, a comparison of the three brittleness curves shows many similarities and a few differences. For example, in the Reitz #2 SWD, outside of the Northview formation where B_7 showed an opposite response to both B_1 and B_2, the other intervals of the Mississippian indicated similar brittleness by each of the brittleness definitions. The Scribner #1 SWD indicated similar brittleness with the exception of the Compton and Kinderhook Formations for the B_7 and B_2 curves. In the Compton and Kinderhook Formations, opposite responses were seen in the curves from B_7 and B_2.

The other purpose of this work is to compare the three brittleness definitions with the interpreted natural fractures from the image log. It is expected that zones of higher brittleness will correlate to zones with higher numbers of natural fractures. Although a reliable estimate of fracture density may not be made due to the bias introduced by the orientation of the wellbore relative to the fracture dip, it is assumed that a reasonable correlation may be made between fracture density and higher number of observed fractures from the image log. The results of this study did not show a strong relationship between the brittleness curves and the number of observed fractures. There are a variety of possible reasons for why this was observed. There are several borehole environmental conditions that could have an effect on the accuracy of the sonic measurements. Borehole rugosity and borehole size are environmental conditions that can influence the reliability of the sonic measurements (Dan Long, personal communication, February 19, 2015). An example of a large borehole size would be the Reitz #2 SWD well, where the well was drilled with a 12.25 inch bit through the Mississippian section. Another influence on the velocities calculated from the Delta T log is fracture density. P and S-wave velocities decrease with increasing fracture density

and will also be influenced by the orientation of the waves to the fractures (Ding et al., 2013). In the Reitz #1, there were observed to be over 190 natural fractures in the Mississippian section. Within the Kinderhook Formation there were a particularly high number of fractures observed from the image log, strongly disagreeing with each of the brittleness equations. As each of the definitions integrate Young's Modulus, derived from sonic velocities, the influence of the fracture density particularly in the Kinderhook Formation may be a reason for the disagreement between the curves and the observed fractures.

There is additional work that may be done to test the usefulness of the brittleness equations. For instance, if core is available for laboratory testing, XRD data could make better estimates of mineralogy and lithology. For this study, lithology was estimated from logs using lithology crossplots. If core were available, fracture toughness could be measured directly in the laboratory. For this study, fracture toughness was estimated using correlations with Young's Modulus found in literature. A more accurate estimate of the fracture density of a particular formation in the subsurface is to detect fractures from an image log run horizontally. Because joints tend to propagate normal to the bedding plane, a borehole parallel to bedding will produce a better assessment of the fracture density.

References

Berendsen, P. and Blair, K.P., 1986, Subsurface structural maps over the Central North American rift system (CNARS), central Kansas, with discussion: Kansas Geological Survey Subsurface Geology Series 8, P-16

Brevetti, J.C., Greer, G.K., Weis B.R., Evaluation of Fractured Carbonates in the Mid-Continent Region., SPWLA 26th Annual Logging Symposium, June 17-20, 1985

Cahill, T. E. (2014). Subsurface sequence stratigraphy and reservoir characterization of the Mississippian limestone (Kinderhookian to Meramecian), south central Kansas and north central Oklahoma (Order No. 1554777). Available from ProQuest Dissertations & Theses Global. (1530192853).

Dolton, Gordon L., Finn, Thomas M. 1989. "Petroleum Geology of the Nemaha Uplift, Central Mid Continent" USGS Report 88-450D

Chang, Soo-Ho., Lee, Chung-In., and Jeon, Seokwan. 2001 Measurement of rock fracture toughness under modes I and II and mixed-mode conditions by using disc-type specimens. Engineering Geology 66 (2002) pg. 79-97

Chiles, J.P., H. Beucher, H. Wackernagel, C. Lantuejoul, P. Elion. 2008. Estimating fracture density from a linear or aerial survey. Proceedings of the VII International Geostatistics Congress, ed. J. Ortiz and Emery. V. 1. P. 535-544

Goodway, B., Varsek, J., and Abaco, C., 2007. Isotropic AVO Methods to Detect Fracture Prone Zones in Tight Gas Resource Plays, Let it Flow—2007 CSPG CSEG Convention, p.585-589

Costello, Daniel, Dubois, M. K., and Dayton, Ryan, 2013. Core to Characterization and Modeling of Mississippian, North Alva Area, Woods and Alfalfa Counties, Oklahoma, *in* Tollefson, Julie (ed.), 2013, Midcontinent Core Workshop: From Source to Reservoir to Seal. Mid-continent Section, American Association of Petroleum Geologists, joint publication by Kansas Geological Survey and Kansas Geological Society, p. 165-174.

Hucka, V., and B. Das (1974), Brittleness determination of rocks by different methods, International Journal of Rock Mechanics and Mining Sciences and Geomechanics Abstract, 11(10), 389-392.

Irwin, G. R., 1956. Onset of Fast Crack Propagation in High Strength Steel and Aluminum Alloys, Sagamore

Jin, X., Shah, S. N., Truax, J. A., & Roegiers, J.-C. (2014, October 27). A Practical Petrophysical Approach for Brittleness Prediction from Porosity and Sonic Logging in Shale Reservoirs. Society of Petroleum Engineers. doi:10.2118/170972-MS

Jin, X., Shah, S. N., Roegiers, J.-C., & Zhang, B. (2014, February 4). Fracability Evaluation in Shale Reservoirs - An Integrated Petrophysics and Geomechanics Approach. Society of Petroleum Engineers. doi:10.2118/168589-MS

Johnson, Kenneth S., 2008. Geologic History of Oklahoma, Oklahoma Geological Survey, Education Publication 9: 2008

Johnson, K.S., 1988 Geologic evolution of the Anadarko basin, in K.S. Johnson, ed., Anadarko basin Symposium: Circular 90, Oklahoma Geological Survey, p. 3-12.

Kluth, C.F., 1986, Plate tectonics of the ancestral Rocky Mountains, in Peterson, J.A., ed., Paleotectonics and sedimentation in the Rocky Mountains region, United States: American Association of Petroleum Geologists Memoir 41, p. 353-369.

Lane, H. R., and DeKeyser, T. L., 1980. Paleogeography of the Late Early Mississippian (Tournaisian 3) in the central and southwestern United States, *in* Fouch, T. D., and Magathan, E. R., (eds.), Paleozoic Paleogeography of west-central United States, Rocky Mountain Section, Society of Economic Paleontologists and Mineralogists, Paleontology Symposium 1, p. 149-162.

Manger, W. L., and Thompson, T. L., 1982. Regional Depositional Setting of Lower Mississippian Waulsortian Mound Facies, Southern Midcontinent, Arkansas, Missouri and Oklahoma, in Bolton, Keith, Lane, H.R., and LeMone, D.V., (eds.), Symposium on the Paleoenvironmental Setting and Distribution of the Waulsortian Facies. El Paso Geological Society and University of Texas at El Paso, p.43-50.

Mazzula, S.J., Wilhite, B.W., and Woolsey, I. W., 2010. Subsurface Mississippian Lithostratigraphy Based on Cores from South Central Kansas and Their Comparison to Outcrops. Abstracts and Programs, Geological Society of America. V. 42, no. 2, p. 42.

Mullen, M., Roundtree, R, Barree, R and Turk, G. 2007. A composite determination of mechanical rock properties for stimulation design (what to do when you don't have a sonic log). Paper SPE 108139 presented at the SPE Rocky Mountain Oil and Gas Technology Symposium, Denver, CO, 16-18 April

Perry, Jr. William J., 1989 Tectonic evolution of the Anadarko Basin Region, Oklahoma. U.S. Geological Survey Bulletin 1866-A

Rickman, R., Mullen, M., Petre, E., Greiser, B., and Kundert, D., 2008. A Practical use of Shale Petrophysics for Stimulation Design Optimization: All Shale Plays are not Clones of the Barnett Shale, SPE Annual Technical Conference and Exhibition, Denver Colorado USA, SPE 115258, p.1-10

Sharma, R. and Chopra, S., 2012. New Attribute for Determination of Lithology and Brittleness, SEG Las Vegas 2012 Annual Meeting, p.1-5

Sih, G. C. 1985. Mechanics and Physics of Energy Density Theory. Theoretical and Applied Fracture Mechanics 4: 157-173

Smith, Dorothy J., 1989. Subsurface Geology of the Northern Shelf of the Anadarko Basin, Oklahoma Geological Survey Circular, pp 245-251

Lili Song, Key Laboratory of Seismic Observation and Geophysical Imaging, Institute of Geophysics, China Earthquake Administration, Yongping Li, Yonghui Wang, Langfang-Research Institute of Petroleum Exploration & Development, CNPC. A Novel Experiment Method of Evaluating the Brittleness of Rock, 2014 SPE

Thornton, W. D., 1964. Mississippian Rocks in the Subsurface of Alfalfa and Parts of Woods and Grant Counties. The Shale Shaker Digest IV, Volumes XII-XIV, p. 117-128.

Ward, L.O., 1965, Mississippian Osage, northwest Oklahoma platform: American Association of Petroleum Geologists Bulletin, v. 49, p. 1562.

Watney, Lynn., Guy, Willard J., Byrnes, Alan P., Characterization of the Mississippian Chat in South-Central Kansas, 2001

Wickham, John; Xinbao, Yu; McMullen, Richard. (2013). Geomechanics of Fracture Density. Unconventional Resources Technology Conference, Paper 1619745.

Whittaker, Barry N., Singh, Raghu N., Sun, Gexin. 1992. Rock Fracture Mechanics Principles, Design and Applications. Developments in Geotechnical Engineering. 71: 349-371

Yang, Y., H. Sone, A. Hows, and M. Zoback (2013), Comparison of Brittleness Indices in Organic rich Shale Formations, paper presented at 47th US Rock Mechanics/Geomechanics Symposium, American Rock Mechanics Association.

Biographical Information

James Martin obtained his Bachelors of Science degree in Geology from the University of Texas at Arlington in 2012. In the fall of 2013, James entered the graduate program at the University of Texas at Arlington with the purpose of studying Petroleum Geology. In May of 2012, James began working with Fairway Resources as a project geologist on their Mississippian Lime project. In August of 2014 the company sold their assets in Oklahoma and James began working as a geologist for Texland Petroleum in Fort Worth, TX. After graduation James will continue to develop as a petroleum geologist with Texland Petroleum.